hν

LEGS

e⁻

BNL

γ

# Scattering of Real Photons and the Structure of Baryons

S. Hoblit and A.M. Sandorfi

Physics Department, Brookhaven National Laboratory
Upton, New York 11973

# Laser Electron Gamma Source

# Brookhaven National Laboratory

# Scattering of Real Photons and the Structure of Baryons

S. Hoblit, A.M. Sandorfi

*Physics Dept., Brookhaven National Lab, Upton, NY 11973*

The leading corrections to point scattering from the proton are characterized by two charge and four spin-polarizability parameters that are sensitive to the proton's internal structure. We review the status of these, focusing on a recent extraction of the backward spin-polarizability, $\gamma_\pi = [-27.1 \pm 2.2(stat + sys)^{+2.8}_{-2.4}(model)] \times 10^{-4} fm^4$, which differs significantly from theoretical expectations.

The transient dipole moments of the proton, induced by the electric and magnetic fields of a photon during Compton scattering, are described by six polarizability parameters that are sensitive to the proton's internal structure. Two of these, the electric ($\bar{\alpha}$) and magnetic ($\bar{\beta}$) polarizabilities, measure the dynamic deformation of the constituent charge and magnetic moment distributions produced by the electromagnetic fields of the photon. The other four arise from the interaction of the photon fields with the constituent spins and so are sensitive to the proton's spin structure [1]. We review here the extraction of a particular linear combination of these spin polarizabilities that characterizes backward Compton scattering [2].

A low-energy expansion (LEX) of the Compton amplitudes to $O(E_\gamma^3)$ which includes the explicit dependence upon the two charge polarizabilities [3], $\bar{\alpha}$ and $\bar{\beta}$, gives a good description of unpolarized photon scattering data up to about 100 MeV [4, 5]. Above this, Compton data deviate from these LEX expectations due to higher order effects. This has been taken into account in the analysis of a number of experiments [6, 7, 8] with the dispersion-theory of L'vov [9], in which the key free parameter is the difference of the charge polarizabilities, $\bar{\alpha} - \bar{\beta}$. This has led to a consistent description of Compton scattering up to single-$\pi$ production threshold ($E_\gamma \sim 150$ MeV lab), with a global average from all data [8] of $\bar{\alpha} - \bar{\beta} = 10.0 \pm 1.5(stat + sys) \pm 0.9(model)$, in units of $10^{-4} fm^3$.

Dispersion integrals relate the real parts of the scattering amplitude to energy-weighted integrals of their imaginary parts. In the L'vov theory [9], these are written as

$$\Re e A_i(\nu, t) = A_i^B(\nu, t) + \frac{2}{\pi} P \int_{\nu_0}^{\nu^{max}} \frac{\nu' \Im m A_i(\nu', t)}{\nu'^2 - \nu^2} d\nu' + A_i^{as}(t), \tag{1}$$

where $\nu = \frac{1}{4M}(s - u)$, M is the nucleon mass, and $A_i^B$ denotes the Born contribution. Here, unitarity fixes the $\Im m A_i$ as products of $\pi$-production multipoles and these are used to calculate the Principal value integral from threshold ($\nu_0$) up to a moderately high energy ($\nu^{max} = 1.5$ GeV). $A_i^{as}$ is the residual asymptotic component. In Regge theory it is expected to be dominated by $t$-channel exchanges and is approximately $\nu$ independent. While four of the six Compton amplitudes are expected to converge

with energy, the two associated with 180° photon helicity-flip (the $A_1$ and $A_2$ amplitudes of [9]) could have appreciable asymptotic parts. In all previous analyses, $t$-channel $\pi^\circ$ exchange was assumed to completely dominate $A_2^{as}$, which is then evaluated in terms of the $F_{\pi^\circ \gamma\gamma}$ coupling. This ansatz left only $A_1^{as}$ to be varied in a fit to data. Since $\bar{\alpha} - \bar{\beta}$ is determined by the $s - u = t = 0$ limit of the $A_1$ amplitude,

$$\bar{\alpha} - \bar{\beta} = -\frac{1}{2\pi} A_1^{nB}(0,0), \tag{2}$$

where the $nB$ superscript denotes the non-Born contributions from the *integral* and *asymptotic* parts of (1), this is equivalent to treating $\bar{\alpha} - \bar{\beta}$ as the single free parameter.

Although this had been accepted as a standard treatment of Compton scattering, we have observed that as higher energy data were added to the fit, the deduced value of $\bar{\alpha} - \bar{\beta}$ dropped [2], becoming even negative when Compton data up to $2\pi$ threshold were included from LEGS and Mainz. We have recently proposed that the weak link here is the *ansatz* of no additional contributions to the asymptotic part of the $A_2$ amplitude beyond those from $\pi^\circ$ $t$-channel exchange. We have model corrections to $A_2^{as}$ with an additional exponential $t$-dependent term having one free parameter, the derivative at $t = 0$. Fitting all modern Compton data, we have found that this addition restores consistency in $\bar{\alpha} - \bar{\beta}$ values deduced from all data up to $2\pi$ threshold [2].

Another consequence of adding a term to $A_2^{as}$ is to alter the expected value for a linear combination of the proton spin polarizabilities that characterizes backward scattering. This *backward spin polarizability*, is a linear combination of the proton spin-polarizabilities of refs. [1] and [10], and is related to their definitions by $\gamma_\pi = -\delta_\pi = (\gamma_1 + \gamma_2 + 2\gamma_4) = \frac{1}{2}(\alpha_2 + \beta_2)$, respectively. In the L'vov dispersion analysis, $\gamma_\pi$ is determined by the $s - u = t = 0$ limits of $A_2$ and $A_5$,

$$\gamma_\pi = -\frac{1}{2\pi M}[A_2^{nB}(0,0) + A_5^{nB}(0,0)]. \tag{3}$$

Evaluation of the dispersion integrals up to 1.5 GeV, together with the ansatz of $t$-channel $\pi^\circ$-exchange for $A_2^{as}$, results in $\gamma_\pi = -36.6$ (in units of $10^{-4} fm^4$), which is dominated by the $\pi^\circ$ contribution, $\frac{1}{2\pi M} A_2^{as} = 44.9$ [9, 11]. (We have included $t$-channel $\eta^0$ exchange, but found this to have a very small effect, -0.7, owing to the large $\eta$ mass and the small $\eta NN$ coupling [12].) A departure of $\gamma_\pi$ from -36.6 would indicate additional unanticipated components in $A_2^{as}(0)$.

We have varied the additional $A_2^{as}$ parameter, together with $A_1^{as}$, in a fit to scattering data to determine the Compton amplitudes. Their $s - u = t = 0$ values then give $\gamma_\pi$ and $\bar{\alpha} - \bar{\beta}$ for the proton.

We summarize here the key components in the LEGS analysis. We have studied Compton scattering up to 350 MeV, and have used the procedure described in [13] of simultaneously fitting $\pi$-production multipoles between 200 and 350 MeV, minimizing $\chi^2$ for both $(\gamma, \gamma)$ and $(\gamma, \pi)$ observables. Outside the fitting interval we have taken the SM95 multipoles from [14]. We have used the same set of $(\gamma, \pi)$ data as in [13], and have included the Compton data from LEGS [13], Mainz [15, 16], SAL

[7, 8], the Max Plank Institute (MPI) [6], Illinois (Ill) [5], and Moscow [4]. (From the Moscow results we have used only the $\sim 90°$ data for reasons discussed in [3].) Relative cross section normalizations, weighted by the systematic uncertainties, were fitted following [17].

In addition to $\gamma_\pi$ and $\bar{\alpha} - \bar{\beta}$ , $\bar{\alpha} + \bar{\beta}$ can also be extracted in terms of the two nonhelicity-flip amplitudes that contribute to 0° scattering, $\bar{\alpha} + \bar{\beta} = -\frac{1}{2\pi}[A_3^{nB}(0,0) + A_6^{nB}(0,0)]$. $A_3^{nB}$ and $A_6^{nB}$ are dominated by the integrals in (1), with only $A_6$ having a small contribution from energies above 1.5 GeV which is varied in fitting the data. Alternatively, $\bar{\alpha} + \bar{\beta}$ can be fixed by the Baldin sum-rule [18],

$$\bar{\alpha} + \bar{\beta} = \frac{1}{2\pi^2} \int_0^\infty \frac{\sigma^{tot}}{\omega^2} d\omega, \qquad (4)$$

where $\sigma^{tot}$ is the total photo-absorption cross section. The right-hand side of (4) has been evaluated [19] from reaction data as $14.2 \pm 0.3$. This has been assumed in previous Compton analyses, although a re-evaluation using recent absorption data has reported $13.7 \pm 0.1$ [20].

| $E_\gamma^{max}$ (MeV) | $\bar{\alpha} + \bar{\beta}$ ($10^{-4}$ fm$^3$) | $\bar{\alpha} - \bar{\beta}$ ($10^{-4}$ fm$^3$) | $\gamma_\pi$ ($10^{-4}$ fm$^4$) |
|---|---|---|---|
| 309 | $13.23 \pm 0.86$ | $10.11 \pm 1.74$ | $-27.1 \pm 2.2$ |
| 309 | 13.7 fixed | $10.45 \pm 1.58$ | $-26.5 \pm 1.9$ |
| 350 | $14.39 \pm 0.87$ | $10.99 \pm 1.70$ | $-25.1 \pm 2.1$ |

Table 1: The global result for the proton polarizabilities (row 1), together with variations from using Eq. 4 as a constraint and from expanding the fit to 350 MeV.

The polarizabilities obtained from the $s - u = t = 0$ values of our fitted amplitudes are summarized in Table 1. The new *global* result (row 1) for $\bar{\alpha} - \bar{\beta}$ from all data below $2\pi$ threshold, $10.11 \pm 1.74(stat + sys)$, is in excellent agreement with the previous average of low energy data [8]. The fitted backward spin-polarizability, $\gamma_\pi = -27.1 \pm 2.2$, is substantially different from the $\pi°$-dominated value of -36.6 that has been implicitly assumed in previous Compton analyses. The extracted $\bar{\alpha} + \bar{\beta} = 13.23 \pm 0.86$ is in agreement with the recent value for the sum rule of (4) from ref. [20]. When $\bar{\alpha} + \bar{\beta}$ is fixed to the value from [20] (row 2), the changes to $\bar{\alpha} - \bar{\beta}$ and $\gamma_\pi$ are negligble. The reduced $\chi^2$ is $964/(692 - 36) = 1.47$ for the full data base, and 1.15 per point for the Compton data alone. (Listed with the results in Table 1 are unbiased estimates of the uncertainties [21]. These are $\sqrt{\chi_{df}^2}$ larger than the standard deviation which encompases both statistical and systematic scale uncertainties.)

We have examined the effect of including Compton data up to 350 MeV, since $2\pi$ production is still quite small below this energy. However, since the polarizabilities enter only the real part of the Compton amplitude, which unitarity forces to zero at the peak of the $P_{33}$ $\Delta$ resonance, the additional

309 - 350 MeV data provide only marginal constraints on the polarizabilities. This expanded fit, row 3 in Table 1, yields a slightly larger $\chi^2_{df}$ (1.57) and extracted polarizabilities which overlap the global results of row 1.

In Table 2 we show the effect of the backward spin-polarizability on the value for $\bar{\alpha} - \bar{\beta}$ when each of the Compton data sets used in the global fit is analysed separately. The results in the third and forth columns assume $\gamma_\pi = -36.6$. Column 3 uses SM95 multipoles from [14] and $\bar{\alpha} + \bar{\beta} = 14.2$ from [19], while the column 4 fits use multipoles from [13] and $\bar{\alpha} + \bar{\beta} = 13.7$ from [20]. In both cases, $\bar{\alpha} - \bar{\beta}$ values deduced from the three high energy data sets (LEGS'97, Mainz'96 and SAL'93) are completely inconsistent with the lower energy measurements. When $\gamma_\pi$ is fixed to -26.5, the fitted value from Table 1 (row 2), consistency among the $\bar{\alpha} - \bar{\beta}$ values is restored (column 5). Significant changes to $\bar{\alpha} - \bar{\beta}$ occur mainly in the high energy results, with the notable exception of the MPI'92 data which were taken at $180°$ where the effect of $\gamma_\pi$ is maximal.

| $(\gamma, \pi)$ multipoles | | SM95 [14] | LEGS [13] | fitted |
|---|---|---|---|---|
| $\gamma_\pi$ ($10^{-4}$ fm$^4$) | | -36.6 | -36.6 | -26.5 |
| $\bar{\alpha} + \bar{\beta}$ ($10^{-4}$ fm$^3$) | | 14.2 | 13.7 | 13.7 |
| Data set | $E_\gamma^{max}$ | | $\bar{\alpha} - \bar{\beta}$ | |
| | (MeV) | | ($10^{-4}$ fm$^3$) | |
| LEGS '97 | 309 | $-0.6 \pm 0.5$ | $1.7 \pm 0.5$ | $9.3 \pm 0.7$ |
| Mainz '96 | 309 | $-1.3 \pm 3.4$ | $-4.3 \pm 3.0$ | $8.4 \pm 4.5$ |
| SAL '93 | 286 | $4.4 \pm 0.6$ | $3.8 \pm 0.6$ | $11.4 \pm 0.8$ |
| SAL '95 | 145 | $10.3 \pm 0.9$ | $10.1 \pm 0.9$ | $11.5 \pm 1.0$ |
| MPI '92 | 132 | $7.3 \pm 2.7$ | $6.9 \pm 2.7$ | $12.5 \pm 3.1$ |
| Moscow '75 | 110 | $8.2 \pm 2.7$ | $8.5 \pm 2.7$ | $11.7 \pm 2.8$ |
| Ill '91 | 70 | $11.1 \pm 4.3$ | $11.1 \pm 4.3$ | $12.1 \pm 4.3$ |

Table 2: Values for $\bar{\alpha} - \bar{\beta}$ deduced from different Compton data sets assuming the previous $\pi°$-dominated value for $\gamma_\pi$ (-36.6) and the new fitted value from Table 1, row 2 ($\gamma_\pi = -26.5$). Pion multipole solutions are listed in the top row, with the last column using the fit of Table 1, row 2, which included all of these Compton data. For the analyses of individual data sets in the ($\gamma_\pi = -36.6$) columns, cross sections were held at their published values, while in the last column normaliztion scales were fixed from the Table 1 fit.

A sample of the high energy data from LEGS, Mainz and SAL is shown in Figure 1, together with calculations that illustrate the sensitivity to $\gamma_\pi$. The data sets are all consistent with each other. (Although in agreement within errors, the Mainz points at $\sim 138°$ from [23] have large uncertainties
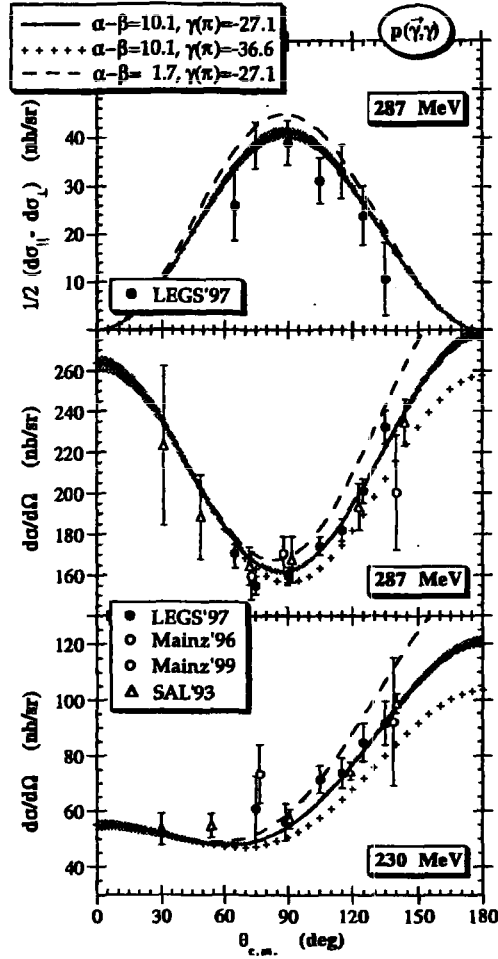
**Figure legend (top panel):**

α−β=10.1, γ(π)=−27.1
α−β=10.1, γ(π)=−36.6
α−β= 1.7, γ(π)=−27.1

p($\vec{\gamma}$,$\vec{p}$)

287 MeV

$\frac{1}{2}$ ($d\sigma_\parallel$ − $d\sigma_\perp$) (mb/sr)

● LEGS'97

$d\sigma/d\Omega$ (mb/sr)

287 MeV

● LEGS'97
○ Mainz'96
○ Mainz'99
△ SAL'93

$d\sigma/d\Omega$ (mb/sr)

230 MeV

0   30   60   90   120   150   180

θ$_{c.m.}$ (deg)

Figure 1: Predictions from dispersion calculations at 230 MeV and 287 MeV, compared to data from refs. [13, 15, 16, 7]. Solid curves are the global fit of Table 1, row 1, with fitting uncertainties indicated by the shaded bands. Plus-signs result from increasing $\gamma_\pi$ and dashes from decreasing $\bar{\alpha} - \bar{\beta}$, as indicated. Dotted curves are predictions from [16, 22].

and were not included in the fits.) The solid curves show our global result, with fitting uncertainties denoted by shaded bands. Curves denoted by plus signs use the old $\pi^\circ$-dominated value for $\gamma_\pi$. The effect of lowering $\bar{\alpha} - \bar{\beta}$ to 1.7 is shown as dashed curves. If both and $\bar{\alpha} - \bar{\beta}$ and $\gamma_\pi$ are changed to 1.7 and -36.6, respectively (the LEGS solution of Table 2, column 4), the predicted cross sections are very close to the solid curves. However, this degeneracy is absent in the $\frac{1}{2}(d\sigma_\parallel - d\sigma_\perp)$ spin-difference, as shown with the LEGS'97 data in the top panel of Figure 1 for $E_\gamma = 287$ MeV. This spin-difference is sensitive to $\bar{\alpha} - \bar{\beta}$ but completely independent of $\gamma_\pi$. Although the limited statistical accuracy of the polarization difference precludes determining $\bar{\alpha} - \bar{\beta}$ from this observable alone, it does provide a useful decoupling of $\bar{\alpha} - \bar{\beta}$ and $\gamma_\pi$.

We have studied the variations in the extracted polarizabilities that result from changing the assumptions used to compute the Compton dispersion integrals, such as the $\pi^\circ$ exchange coupling,

multipion photoproduction, and the form of asymptotic contributions [9], particularly the new term added to $A_2^{a'}$, as well as the parameterization of the fitted $(\gamma, \pi)$ amplitude [13]. Combining these model uncertainties in quadrature leads to our final results:

$$\gamma_\pi = [-27.1 \pm 2.2(stat + sys)^{+2.8}_{-2.4}(model)] \times 10^{-4} \text{ fm}^4,$$

$$\bar{\alpha} - \bar{\beta} = [10.11 \pm 1.74(stat + sys)^{+1.22}_{-0.86}(model)] \times 10^{-4} \text{ fm}^3,$$

$$\bar{\alpha} - \bar{\beta} = [13.23 \pm 0.86(stat + sys)^{+0.20}_{-0.49}(model)] \times 10^{-4} \text{ fm}^3.$$

A recent analysis using a different set of dispersion relations to calculate the real parts of the Compton amplitudes has obtained a similar value for $\gamma_\pi$ [24].

In figure 2 Compton cross sections are plotted at the peak of the $\Delta$. At resonance, the real part of the scattering amplitude vanishes, removing any dependence in the cross section to the polarizabilities since these enter only the real parts of the amplitude. Also shown is an identical calculation only replacing the pion multipoles with the HDT multipoles of ref. [25]. The resulting prediction is shown in figure 2 as the dashed curve and illustrates the sensitivity to the pion multipole solution. The lower values of the dashed curve have their origin in the lower $(\gamma, \pi)$ cross sections from Mainz that were used in fixing the HDT multipole solution [13, 25].
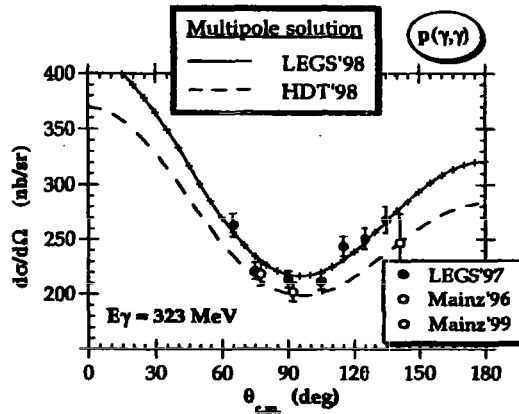


Figure 2: The solid curve shows the fit of Table 1, row 3, at 323 MeV, the peak of the $\Delta$. The plus sign curve has the same meaning as in figure 1. The dashed curve is the prediction repeated using the HDT pion multipoles of [25].

To examine the sensitivity of the deduced value of $\gamma_\pi$ upon the $(\gamma, \pi)$ multipole solution we have refit the Compton data from LEGS, Mainz and SAL [13, 15, 16, 7] using the HDT multipoles from [25] and the SP97k solution from VPI [14]. The results are listed in the first row of Table 3. These two solutions were fitted to the Mainz and Bonn $(\gamma, \pi)$ data. If $\gamma_\pi$ is fixed to -37, the Compton predictions using either of these are lower than the plus-sign curves of Fig. 1 and 2. So a value for $\gamma_\pi$ even higher than -27 is needed to raise the predictions up to the scattering data.

| | $(\gamma, \pi)$ multipoles | | |
|---|---|---|---|
| | LEGS '98 | HDT '98 | SP97K |
| $m_\sigma = 600$ | $\gamma_\pi = -27.1 \pm 2.2$ | $\gamma_\pi = -21.4 \pm 0.9$ | $\gamma_\pi = -20.9 \pm 0.8$ |
| $\delta = 37$ | $m_\sigma = 217 \pm 6$ | $m_\sigma = 82 \pm 20$ | $m_\sigma = 58 \pm 23$ |

Table 3: Results of fits to Compton data up to $2\pi$ threshold [13, 15, 16, 7] using different $(\gamma, \pi)$ multipoles from [2, 25, 14]. In all cases, $\bar{\alpha} - \bar{\beta}$ is fixed at 10 and $\bar{\alpha} + \bar{\beta}$ to 13.7 $(10^{-4} \, \text{fm}^3)$. For fits in the first row, the $\sigma$ mass was fixed at 600 MeV and $\gamma_\pi$ was varied. For the second row, $\gamma_\pi$ was fixed at -37 $(10^{-4} \, \text{fm}^3)$, and the $\sigma$ mass was varied. The $\chi^2$/point for all fits is less than 1.4.

There has been a recent suggestion [26] of a possible way to fit the Compton data while leaving the value of $\gamma_\pi$ at its $\pi^\circ$-dominated expectation of -37. The asymptotic part of the $A_1$ amplitude is assumed to be dominated by $t$-channel $\sigma$-exchange, with $\sigma$ being the correlated s-wave $2\pi$ object required in analyses of N-N scattering [9]. Since its couplings are poorly known they are simple treated as a free parameter in fitting $A_1^{as}$. In this procedure we have set the $\sigma$ mass to 600 MeV, an average of several N-N analyses. The authors of [26] have pointed out that reducing $m_\sigma$ changes the $t$-dependence in such a way as to raise the back angle cross section so that one might be able to reconcile predictions with data in this way while leaving $\gamma_\pi$ fixed at -37. We have investigated this suggestion, and the results of refitting the Compton data, varying $m_\sigma$ while fixing $\gamma_\pi = -37$, are shown in row 2 of Table 3. Good fits can indeed be obtained in this way, but only with a value for $m_\sigma$ that is substantially less than the mass of two pions.
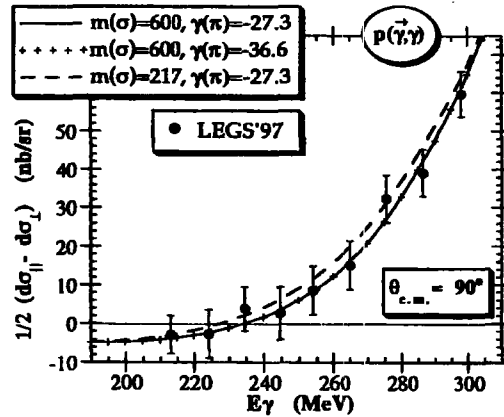


Figure 3: Predictions from the LEGS multipoles for the Compton spin difference $\hat{\Sigma} = \frac{1}{2}(d\sigma_\parallel - d\sigma_\perp)$ for various combinations of $m_\sigma$ and $\bar{\alpha} - \bar{\beta}$. The data are from [13].

Some additional information on the scenario of a lower $\sigma$ mass comes from the $\hat{\Sigma} = \frac{1}{2}(d\sigma_\parallel - d\sigma_\perp)$ spin difference. Since this observable is completely independent of the $A_2$ amplitude is free of the

$\gamma_\pi$ versus $m_\sigma$ ambiguity. The data for $\hat{\Sigma}(90°)$ is shown in the top panel of figure 1 and in figure 3. Although the error bars are still appreciable compared with the separation between curves, the value of $\chi^2/\hat{\Sigma}$-point is noticeably lower for the $m_\sigma = 600$ MeV solution (1.25), as compared to that for $m_\sigma = 217$ MeV (1.45). On the whole, drastic reductions of the $m_\sigma$ does not seem a realistic alternative.
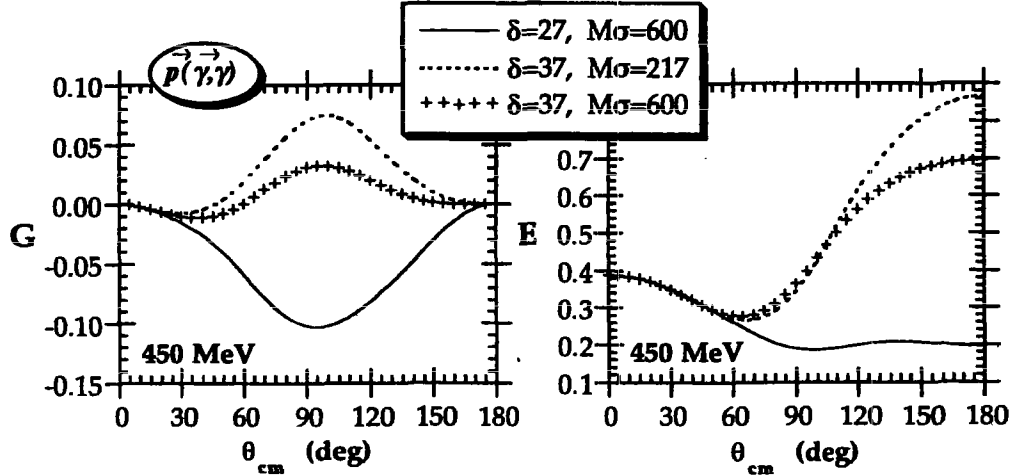


Figure 4: Predictions from the LEGS multipoles for Compton double-polarization observables, $G$ with linearly-polarized beam and $E$ with circularly-polarized beam, both on longitudinally-polarized proton targets.

A value of $\gamma_\pi$ appreciably higher than -37 is difficult to accommodate within existing theories. Although $\chi$PT cannot be expected to directly predict Compton observables at the high energies included in these dispersion analyses, it should be able to reproduce the polarizabilities obtained by evaluating the fitted amplitudes at $s - u = t = 0$. Nonetheless, existing $O(\omega^3)$ calculations remain close to the $\pi°$-dominated value [27]. Since our result for $\gamma_\pi$ would indicate some new contribution from the low-energy spin structure of the proton, it is highly desirable to verify this in some independent way. As pointed out in [26], beam-target double-polarization observables are sensitive to both $\gamma_\pi$ and the $\sigma$ mass. In Fig. 4 we plot angular distributions predicted with the LEGS multipoles for two such observables: the $G$-asymmetry obtained with linearly polarized beam on longitudinally polarized protons (the $\Sigma_{1z}$ observable in [26]), and the $E$-asymmetry from circularly polarized beam on a longitudinally polarized target ($\Sigma_{2z}$ in [26]). Checking either the $\gamma_\pi = -37$, or reduced $m_\sigma$ predictions should be quite straight forward, and measurements of these quantities are expected in the near future.

# References

[1] S. Ragusa, Phys. Rev. D **47**, 3737 (1993).

[2] J. Tonnison, A.M. Sandorfi, S. Hoblit and A.M. Nathan, Phys. Rev. Lett. **80**, 4382 (1998).

[3] V.A. Petrun'kin, Sov. J. Part. Nucl. **12**, 278 (1981).

[4] P.S. Baranov *et al.*, Sov. J. Nucl. Phys. **21**, 355 (1975).

[5] F.J. Federspiel *et al.*, Phys. Rev. Lett. **67**, 1511 (1991).

[6] A. Zieger *et al.*, Phys. Lett. B **278**, 34 (1992).

[7] E.L. Hallin *et al.*, Phys. Rev. C **48**, 1497 (1993).

[8] B.E. MacGibbon *et al.*, Phys. Rev. C **52**, 2097 (1995).

[9] A.I. L'vov, Sov. J. Nucl. Phys **34**, 597 (1981); A.I. L'vov *et al.*, Phys. Rev. C **55**, 359 (1997).

[10] D. Babusci, G. Giordano, and G. Matone, Phys. Rev. C **55** 1645 (1997).

[11] D. Drechsel *et al.*, Phys. Lett. B **420**, 248 (1998).

[12] T. Feuster and U. Mosel, Phys. Rev. C **58**, 457 (1998).

[13] LEGS Collaboration, G. Blanpied *et al.*, Phys. Rev. Lett. **79**, 4337 (1997); **76**, 1023 (1996).

[14] R. Arndt, I. Strakkovsky, and R. Workman, Phys. Rev. C **53**, 430 (1996).

[15] C. Molinari *et al.*, Phys. Lett. B **371**, 181 (1996).

[16] J. Peise *et al.*, Phys. Lett. B **384**, 37 (1996).

[17] G. D'Agostini, Nucl. Instrm. Methods Phys. Res., Sect. A **346**, 306 (1994).

[18] A.M. Baldin, Nucl. Phys. **18**, 310 (1960).

[19] M. Damashek and F.J. Gilman, Phys. Rev. D **1**, 1319 (1970).

[20] D. Babusci, G. Giordano, and G. Matone, Phys. Rev. C **57**, 291 (1998).

[21] J.R. Wolberg, *Prediction Analysis* (Van Nostrand Co., New York, 1967), pp. 54-66.

[22] A. Hünger *et al.*, Nucl. Phys. **A620**, 385 (1997).

[23] F. Wissmann et al., Mainz preprint, submitted to Nucl. Phys. (June, 1999); private communication.

[24] D. Drechsel, M. Gorchtein, B. Pasquini and M. Vanderhaeghen, hep-ph/9904290.

[25] O. Hanstein, D. Drechsel and L. Tiator, Nucl. Phys. **A632**, 561 (1998).

[26] D. Babusci, G. Giordano, A. Lvov, G. Matone and A. Nathan, Phys. Rev. **C58**, 1013 (1998).

[27] T. Hemmert, B. Holstein, J. Kambor and G. Knöchlein, Phys. Rev. **D57**, 5746 (1998).